JCTC Journal of Chemical Theory and Computation

pubs.acs.org/JCTC Article

Electronic Polarizability Tunes the Function of the Human Bestrophin 1 Cl^- Channel

Linda X. Phan, Aaron P. Owji, Tingting Yang, Jason Crain, Mark S.P. Sansom, and Stephen J. Tucker*

Cite This: J. Chem. Theory Comput. 2025, 21, 933−942 Read Online

ABSTRACT: Mechanisms of anion permeation within ion channels and nanopores remain poorly understood. Recent cryo-electron microscopy structures of the human bestrophin 1 Cl^- channel (hBest1) provide an opportunity to evaluate ion interactions predicted by molecular dynamics (MD) simulations against experimental observations. Here, we implement the fully polarizable force field AMOEBA in MD simulations on different conformations of hBest1. This force field models multipole moments up to the quadrupole. Using this approach, we model key biophysical properties of the channel that can only be simulated when electronic polarization is included in the molecular models and show that Cl^- permeation through the neck of the pore is achieved through hydrophobic solvation concomitant with partial ion dehydration. Furthermore, we demonstrate how such polarizable simulations can help determine the identity of ion-like densities within high-resolution cryo-EM structures and demonstrate that neglecting polarization places Cl^- at positions that do not correspond to their experimentally resolved location. Overall, our results demonstrate the importance of including electronic polarization in realistic and physically accurate models of biological systems, especially channels and pores that selectively permeate anions.

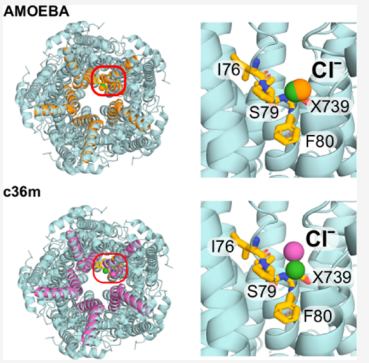

INTRODUCTION

Ion channels are nanoscale pore-forming membrane proteins that enable the rapid and selective passage of ions across a membrane. Their activity and function are central to the regulation of physiological processes, from cell signaling and the control of pH balance to muscle contraction and brain function.[1,2] Chloride ions are the most abundant anions in living organisms. Since dysfunction of associated Cl^- channels is known to result in a variety of disease states, these proteins represent attractive therapeutic targets.[3] However, the underlying mechanisms of Cl^- permeation and selectivity in these channels remain under-explored relative to their cation counterparts, which is partly a consequence of their weak selectivity.[4] It is therefore of great interest to explore the mechanisms of anion permeation in such channels and thoroughly assess the essential physics needed for an accurate functional annotation.

Studies suggest that Cl^- can form favorable interactions with hydrophobic interfaces ranging from simple air/water interfaces to more complex protein interfaces.[5−7] The anisotropy of such interfaces induces a dipole in the Cl^- that is otherwise not present in the bulk. Interactions between the induced dipole and surrounding water molecules compensate for the partial dehydration of Cl^- as it adsorbs at the interfacial layer and comes into direct contact with the hydrophobic interface.[8] This phenomenon can be observed across the halide subset of the Hofmeister series, i.e., $F^- < Cl^- < Br^- < I^-$, whereby the softer, more polarizable anions are more prone to dehydration and localize at the interface.[9]

Anion interactions with aromatic edges are also a well-established phenomenon[10−12] and have more recently been recognized to play important roles in buried regions of proteins.[11,13] Additionally, the ion conduction pathway within some anion channels can be composed of aromatic residues, such as phenylalanine. Known structures of anion channels that exploit this include the mechanosensitive Cl^- channel, Flycatcher1 (FLYC1), where the narrowest constriction (∼2.8 Å radius) is created by a ring of phenylalanine side chains;[14] the slow anion channel (SLAC1), which is occluded by a highly conserved phenylalanine residue responsible for channel gating (<2 Å)[15] and the mechanosensitive channel of small conductance from *Escherichia coli* (EcMscS) in which phenylalanines appear to constitute the hydrophobic gate (∼4 Å).[16] However, although such anion-aromatic interactions are readily observed, the degree to which dilation is required for anion passage in the presence of pore-lining phenylalanine residues is variable and is only partially understood. Therefore, there is a need for further biophysical characterization to better understand the functional roles of such pore-lining aromatics and their contributions toward anion permeation.

Received: August 8, 2024
Revised: December 23, 2024
Accepted: December 26, 2024
Published: January 3, 2025

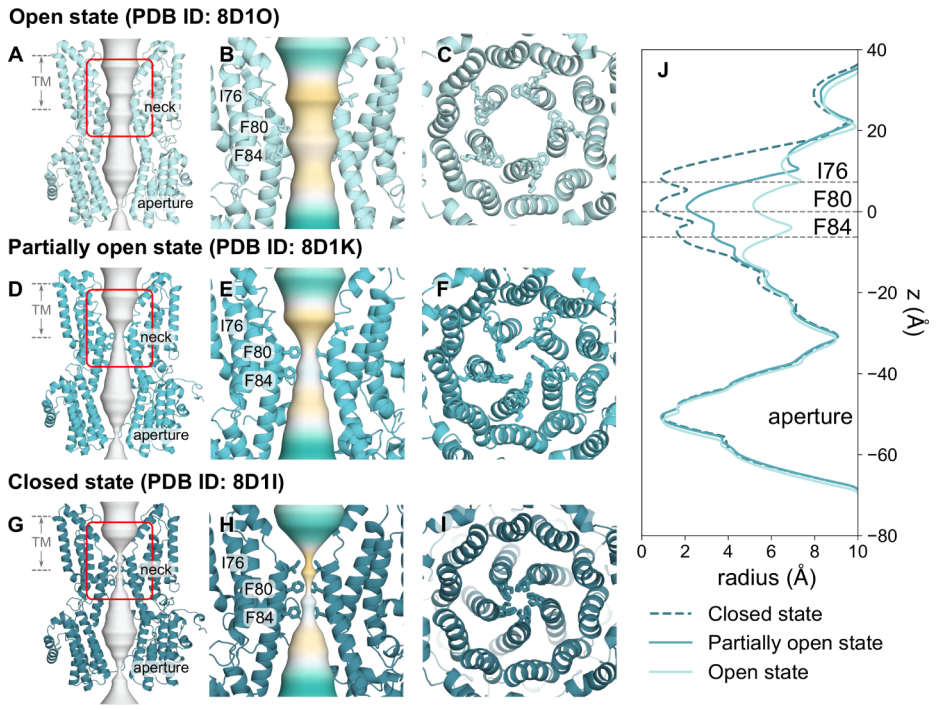

Figure 1. Cryo-EM structures of hBest1 in the open and "partially open" states. A Open state hBest1 (PDB ID 8D1O), D partially open state hBest1 (PDB ID 8D1K) and G closed state hBest1 (PDB ID 8D1I) structures visualized with ion permeation pathway in white. The red box indicates the neck region—a constriction composed of three hydrophobic pore-facing residues. A zoomed in focus on this transmembrane neck region of the B open state, E partially open state, and H closed state structures are illustrated with their ion permeation pathway colored by hydrophobicity with pale brown corresponding to maximum hydrophobicity and green corresponding to maximum hydrophilicity. Top-down view of the C open state neck, F partially open state, and I closed state hydrophobic neck and region of interest in this study. J Pore radius profiles of the open, partially open, and closed states.

Cryo-electron microscopy (cryo-EM) is a powerful structural technique that has revolutionized the field of structural biology. Recent technological improvements in sample treatment, grid preparation, microscope hardware, and image processing have made it achievable to obtain high-resolution maps better than 3 Å.[17] Despite these advancements, there are several caveats, such as radiation damage resulting in lower signal-to-noise ratios, protein denaturation, and beam-induced sample movement, which all present limitations to achieving even higher resolutions.[18] The resolution of single-particle cryo-EM is also often insufficient to provide detailed information on small molecules or bound ligands, such as water or ions, which require a resolution of at least 2.5 Å,[19] and so it can be difficult to differentiate and interpret these small densities with confidence when using this technique. Molecular dynamics (MD) simulations can extend the capabilities of cryo-EM by capturing the conformational variability and short-lived states. Furthermore, MD simulations can assist in the assignment and interpretation of cryo-EM data to access improved atomic resolution structures.[20]

The majority of MD simulations employ pairwise additive force fields that model electrostatic interactions as Coulombic forces between fixed point charges.[21] These force fields do not capture the effects of induced polarization that arise from redistributions of charge density in response to local field gradients. This becomes problematic for modeling systems that involve polarizable moieties, such as aromatic residues and polarizable anions. Charge-scaling methods, such as the prosECCo75[22−24] and NBFIX[25,26] approaches applied to existing pairwise additive force fields, aim to improve molecular interactions by more accurately capturing the effects of induced polarization, leading to better agreement with experimental data. Furthermore, a number of biomolecular force fields have recently been developed to explicitly capture induced polarization. Among these, two of the most widely employed are the AMOEBA force field,[27] which models atomic monopoles through to quadrupole moments within a classical MD framework, and the CHARMM Drude force field,[28,29] which uses massless Drude oscillators to displace charge from atomic centers. These force fields provide new and improved levels of predictive power over nonpolarizable force fields and are increasingly being used to investigate proteins;[6,30,31] however, they incur additional computational costs.

An example where modeling polarization may be vital is in the study of Cl^--selective ion channels. Due to the weakly polarizable nature of Cl^-,[32] realistic behavior is subtle and often difficult to capture. A suitable model is the Bestrophin channels, a family of calcium-activated Cl^- channels (CaCCs) where many questions still remain.[33,34] Four paralogs (Best1−4) have been identified in eukaryotes, which are responsible for a diverse range of functions.[34] The best-known physiological role of Best1 is in the eye, where disease-causing mutations lead to retinal degenerative disorders called bestrophinopathies. The structures of the bestrophin channels contain two key constrictions in the ion conduction pathway. A permeating ion from the extracellular side will first encounter the neck region, which is a gate composed of three hydrophobic residues (I76, F80, and F84) that are highly conserved across homologues. After passing this gate, the ion will traverse the interior of the cytosolic vestibule, followed by a second, shorter constriction at the cytosolic exit, called the aperture, which displays significant divergence across paralogs.[34] Together, the

https://doi.org/10.1021/acs.jctc.4c01039
J. Chem. Theory Comput. 2025, 21, 933−942

neck and aperture are both thought to comprise part of the gating mechanism for bestrophin channels, although their relative contribution to gating and/or Cl^- selectivity remains unclear.[34−37]

Comparison of the human Bestrophin 1 channel (hBest1) in a fully open state (PDB ID 8D1O, 2.4 Å resolution) (Figure 1A−C and G) with a "partially open neck" conformation (PDB ID 8D1K, 2.3 Å resolution) (Figure 1D−G)[36] reveals a conformational change in the pore-facing residues of the hydrophobic neck (Figure 1B,E). In particular, the three states differ in the radius profile in the neck of the pore, with minimum HOLE radii of 0.5 Å in the closed state, 4.5 Å in the open state, and 2 Å in the 8D1K structure.[36] The 8D1K structure has therefore been (provisionally) designated as "partially open" given that the radius of a fully hydrated chloride ion ∼4 Å[38] and we refer to this as the partially open state in this paper. This difference allows us to probe the mechanisms of ion permeation and selectivity as well as the conformational pathway to channel opening.

In this study, we therefore explore the effect of electronic polarization on hBest1 function by implementing fully polarizable force fields to examine the behavior of Cl^- within the neck region. Here, we present an example of how such force fields provide novel detailed insights into channel function and the behavior of Cl^- in the neck of hBest1. They also reveal the roles of aromaticity and pore asymmetry in ion permeation. In particular, phenylalanine side chains are seen to undergo a conformational change that enables edge-on interactions with a partially dehydrated Cl^- during permeation. Crucially, we also show that models which include realistic polarization can be used to interpret ambiguous ion-like densities observed in experimental high-resolution cryo-EM structures, thus enabling more accurate functional annotation.

METHODS

Structural Model and System Preparation. Cryo-EM structures of human Bestrophin 1 (hBest1) in the Ca^{2+}−bound open state (PDB ID 8D1O, 2.4 Å resolution) and the hBest1 Ca^{2+}-bound partially open neck state (PDB ID 8D1K, 2.3 Å resolution)[36] were obtained from the Protein Data Bank (PDB). Due to the methodological and high computational demands for implementing explicitly polarizable force fields, we reduced the protein structures to include the pore-lining segments spanning most of the transmembrane domain. The protein fragments were composed of residues 56 to 99, which encompass the neck region of interest (residues I76, F80, and F84) (Figure S1). Truncation at these residues was chosen as they span the transmembrane domain, with the neck region of interest located centrally within this area. The truncation was selected to minimize the effects of reducing the system on the neck region of interest while keeping the system computationally feasible. Protein fragment systems were solvated in a 0.5 M NaCl solution and were prepared using the CHARMM-GUI protocol.[39]

Nonpolarizable Molecular Dynamics. MD simulations employing a nonpolarizable force field were performed in GROMACS[40] version 2021 using the CHARMM36m (c36m) force field in conjunction with the mTIP3P water model. Protein fragment systems were first subjected to energy minimization, followed by a 2 ns NVT equilibration period. Simulations in the NPT ensemble were conducted for 100 ns, whereby the first 20 ns of each simulation were discarded as an equilibration. Therefore, the final 80 ns of the simulation were used for analysis. Simulations were carried out using the leapfrog integrator with a time step of 2 fs. The temperature was maintained at 310 K using the Nosé−Hoover thermostat[41] with a time coupling constant of 1.0 ps. The pressure was maintained at 1 bar using the Parrinello−Rahman barostat[42] with a time coupling of 5.0 ps. Short-range electrostatics were treated with the Verlet cutoff scheme with a cutoff at 1.2 nm, and long-range electrostatics were treated with the particle mesh Ewald (PME) algorithm.[43] The LINCS algorithm[44] was used to constrain H-bonds. Backbone atoms were placed under harmonic restraints with a force constant of 1000 kJ/mol/nm^2 to prevent the structures from deviating too much from the experimental coordinates. Three independent repeats were carried out for each system.

Polarizable Simulations Molecular Dynamics. Fully polarizable force field simulations were carried out in OpenMM 7.4.2 (www.openmm.org) and all components in the system were modeled with the AMOEBA polarizable force field using the amoeba2013 parameter set.[45] Starting configurations for these simulations were obtained from the end of the NVT ensemble equilibration period using c36m, as described above. Simulations were then set up following a similar procedure to a method described previously (https://github.com/Inniag/openmm-scripts-amoeba).[6] Two independent repeats were carried out for polarizable force field simulations. AMOEBA force field simulations proceeded by performing 1000 steps of energy minimization to resolve any divergent energies due to the induced dipoles. The production run was simulated for 60 ns, with the first 10 ns of the simulation discarded for equilibration; therefore, the final 50 ns were used for analysis. Time integration was performed using the r-RESPA multiple time step integration algorithm[46] with an inner time step of 0.25 fs and an outer time step of 2 fs. The temperature was maintained at 310 K using the Andersen thermostat, and pressure was maintained at 1 bar using the isotropic Monte Carlo barostat. Electrostatic multipole interactions were evaluated by the PME method with a real-space cutoff of 8 Å and a tolerance of 5×10^{-4} and a fifth-order B-spline interpolation. VdW interactions were calculated explicitly up to a distance of 12 Å, and interactions beyond this cutoff were treated with an analytical long-range dispersion correction. All C_α atoms were placed under a harmonic restraint with a force constant of 1000 kJ/mol/nm^2 to prevent the protein from deviating from the experimental structure.

Binding Site Identification and Analysis. Interactions of Cl^- with each protein structure, binding site detection, and quantification were calculated using PyLipID (https://github.com/wlsong/PyLipID).[47] Binding sites were defined by sites with four or more residues that form Cl^- contacts and by a single cutoff scheme for which Cl^- ions were considered bound if they resided within 4 Å. This interaction distance was determined by calculating the radial distribution function (RDF) between Cl^- and oxygen atoms from water molecules in bulk solvent using the c36m and AMOEBA force fields (Figure S2). Alignment and visualization of structures were achieved using PyMOL (https://pymol.org/2/). Trajectory analysis was performed using MDAnalysis[48,49] and GROMACS analysis tools.[40] The pore radius profiles were obtained using CHAP (www.channotation.org).[50]

RESULTS AND DISCUSSION

To probe the role of the conserved neck region in bestrophin channels, we have performed atomistic MD simulations of

https://doi.org/10.1021/acs.jctc.4c01039
J. Chem. Theory Comput. 2025, 21, 933−942

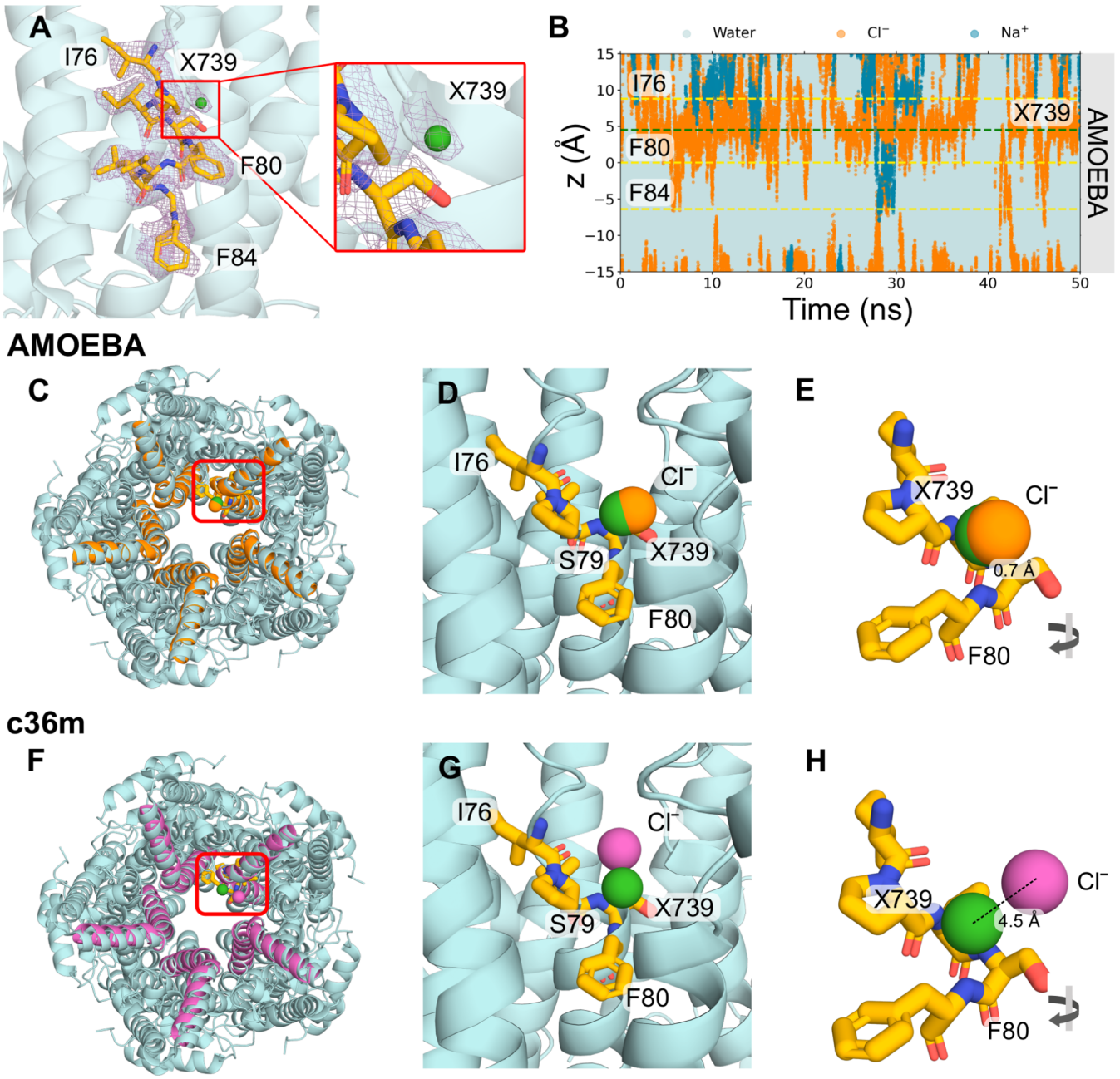

Figure 2. Cl^-binding site analysis. (A) Close-up representation of neck residues (I76, F80 and F84) from a single chain highlighted in licorice representation of the open state structure (PDB ID 8D1O). The cryo-EM densities are shown as a mesh representation in purple at a contour level of 1.9σ visualized in PyMOL. A panel is zoomed in on the nonprotein ion-like density in proximity to F80 labeled as X739, which corresponds to the water molecule HOH739 in the PDB. (B) The trajectories of water (cyan), Na^+ (dark blue) and Cl^- (orange) ions in z-coordinates as a function of time within the neck region of the pore. The plot indicates that Cl^- tends to cluster in a region between I76 and F80. The green dashed line represents the location of X739 from the experimental structure. AMOEBA force field simulations: Top-down view of the protein fragment in (C) AMOEBA (orange) or (F) c36m (magenta) aligned to the full protein structure (cyan). The location of X739 is indicated by the green sphere. The top detected binding pose identified with PyLipID shows (D) significant overlap between the AMOEBA Cl^- (orange sphere) and X739, indicating this site likely functions as a Cl^- binding site or (G) the c36m Cl^- (magenta sphere) shares no overlap with X739. (E, H) A rotated view showing the distance of the respective Cl^- to X739 in the experimental structure.

fragments from hBest1 containing the neck region and pore-lining sections from both the fully open (PDB ID 8D1O) and partially open neck states (PDB ID 8D1K). These fragments consisted of residues 56 to 99 from the full protein and were simulated in a 0.5 M NaCl solution (Figure S1). Previous studies of reduced systems of ion channels focusing on isolated sections have shown that they can provide an accurate representation of the dynamics within the original protein.[6,51,52] While these simplified systems may not fully capture the physiological context of bestrophin, nonetheless, they still offer valuable insights into specific interactions of interest within a more biologically relevant framework.

To validate the protein fragment, we performed simulations of the full protein embedded in a lipid bilayer compared with that of the protein fragment and analyzed the average water density. The resulting profiles are similar, and the average

https://doi.org/10.1021/acs.jctc.4c01039
J. Chem. Theory Comput. 2025, 21, 933−942

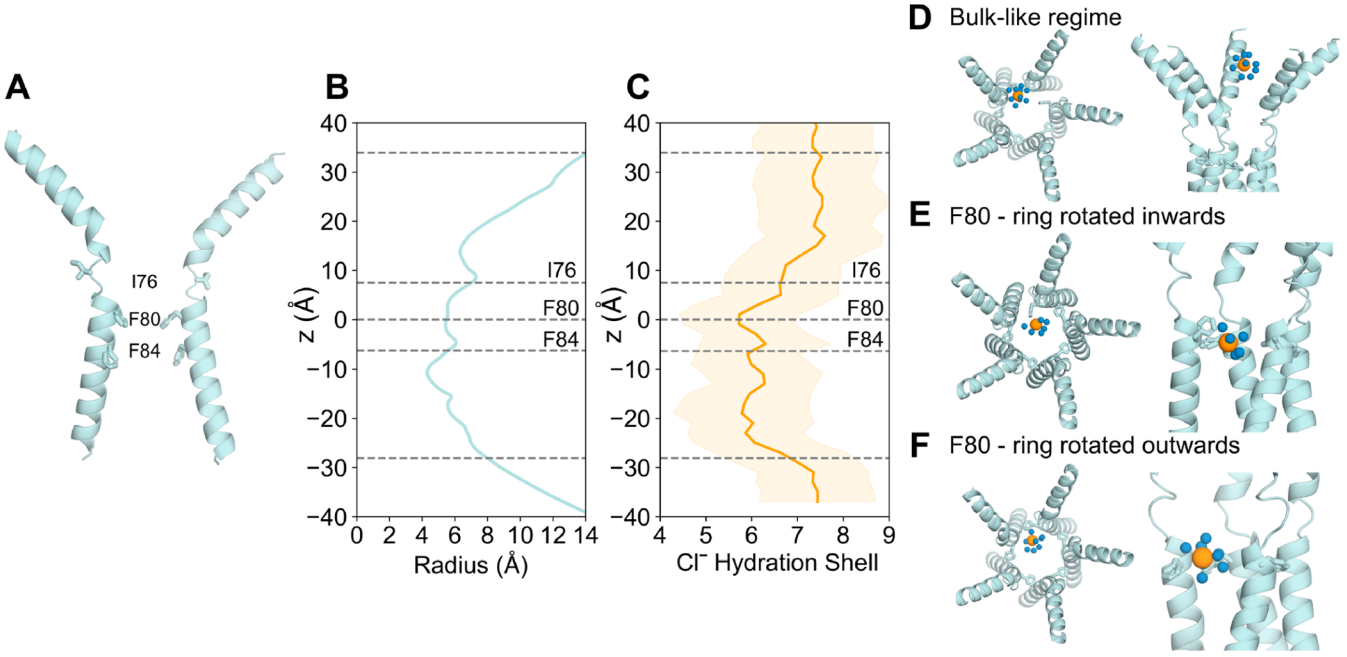

Figure 3. The role of water in Cl^- permeation in the open state AMOEBA simulations. (A) Cross-section schematic of the protein fragment of the open state bestrophin (PDB ID 8D1O) with the neck residues illustrated in licorice representation. (B) The pore radius profile of the open state fragment. The outer gray dashed lines represent the extent of the protein and the central lines indicate the z-location of the neck residues where z is the distance down the axis of the pore and $z = 0$ corresponds to the C_α of F80. (C) The first hydration shell of Cl^- as a function of z. The shaded orange region represents the standard error in hydration number at a given z. Snapshots exemplifying the first hydration shell (blue spheres) of Cl^- (orange spheres) in (D) the bulk-like water regime within the protein fragment. (E) The partial loss of hydration shell due to anion-π interactions with the aromatic rings of F80 rotated inward toward the pore axis. (F) The partial loss of Cl^- hydration due to anion−π interactions with the aromatic rings of F80 oriented outward as in the experimental structure conformation.

water density remains close to bulk outside the neck region (Figure S3A). This provides confidence that the protein fragments in our reduced system offer a representative model of the fully open and hydrated pore from the full protein. Furthermore, we assessed the RMSDs of the pore-lining side chains from the neck residues (I76, F80, F84) to evaluate their structural stability. The side chains in the protein fragment were considered structurally stable with fluctuations <2 Å (Figure S3B). The system contains aromatic residues and polarizable ions and therefore justifies the use of fully polarizable force fields, such as AMOEBA. However, with added complexity comes increased computational costs, hence the need to reduce the system size to make the simulations computationally feasible.

Interpretation of Cryo-EM Densities as Anion Binding Sites from Fully Polarizable MD Simulations. In the experimental structure of the open state hBest1, a number of nonprotein, ion-like densities have been observed, which have been modeled as water molecules in the published structure. A set of these water molecules (corresponding to HOH739 and HOH539 in the PDB) are located within the neck region and appear to bind to the helix dipole[53] at a distance of 3.2 Å to the backbone NH of F80 of each chain (Figure 2A). Similar nonprotein densities are also observed consistently in proximity to the helix dipole in the open state structure of human bestrophin 2 (hBest2) (PDB ID 8D1N). Due to experimental limitations, there is ambiguity in the molecular identity of these densities. Assessment of the local chemistry and comparisons with known bromide binding sites from anomalous scattering studies of a Best1 homologue[54] suggest the location of these densities is comparable to the putative water molecules in the hBest1 structure. Therefore, it has been suggested that this site could possibly serve as a Cl^- binding site. Here, we have used the AMOEBA force field to explore the possibility that these densities could instead be representative of Cl^-. We refer to the density X739 as the ion-like density previously labeled as a water molecule (HOH739) in the PDB.

Analysis of the z-positions of ions and water as a function of time revealed that the open state neck is wetted and permeable to ions. The average total number of water molecules within the permeation pathway is ∼785 ± 20, as calculated by CHAP.[50] There is a clear accumulation of Cl^- in the region between I76 and F80 of the neck (indicated by the dense orange region in Figure 2B surrounding the green line representing X739). Cl^- can also be observed to permeate the neck, as Cl^- can be seen to occupy z-positions across I76 to F84. Na^+ can be observed to be largely excluded from the neck region; however, a small fraction may traverse the neck (e.g., Figure 2B at ∼28 ns). In contrast, the c36m simulations (Figure S4) show no distinct clustering of Cl^- between residues I76 and F80, and additionally, Na^+ appears to be more readily able to permeate. Our simulations do not provide sufficient sampling for studying ion conductance ratios.

To pinpoint precisely where Cl^- is clustering in three dimensions, we have used the computational tool PyLipID, which is capable of analyzing protein−ligand interactions.[47] Taking the top-ranked binding pose for the detected binding site, we focused on interactions of a single chain and aligned the simulated fragment structures with the original PDB structure (chain E and HOH739) for comparison (Figure 2C). The results of the AMOEBA simulations correlate very well with the cryo-EM densities. A significant overlap can be seen between the Cl^- and the water molecule (X739) modeled in

https://doi.org/10.1021/acs.jctc.4c01039
J. Chem. Theory Comput. 2025, 21, 933−942

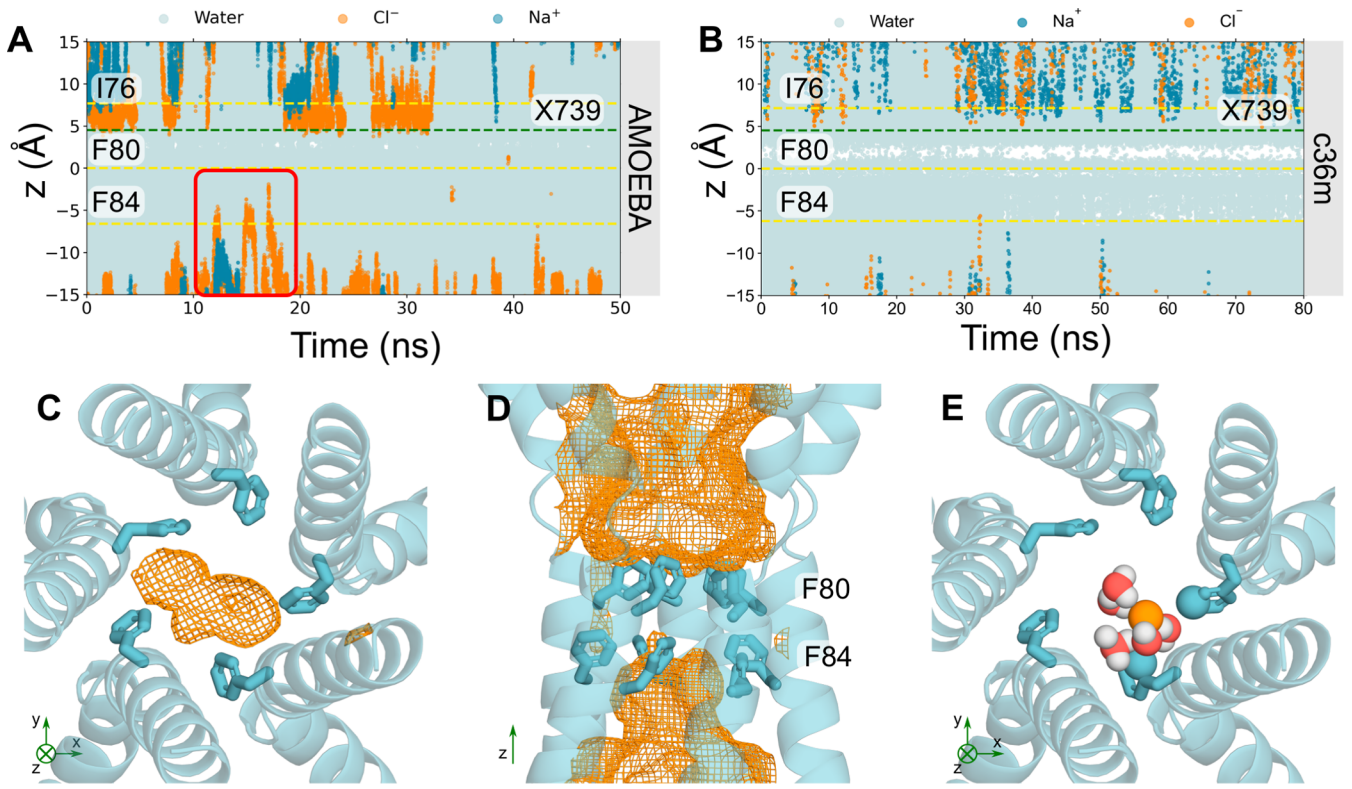

Figure 4. Analysis of the partially open state Trajectories of water (cyan), sodium (dark blue) and Cl^- (orange) ions in z-coordinates as a function of time within the neck region of the partially open state pore (PDB ID 8D1K) using A the AMOEBA force field or B c36m force field. The red box in A highlights a Cl^- that can occupy locations above F84 in the neck whereas nearly no ions can be seen in B with c36m. C Bottom-up view of F84 of the partially open state neck. The volume that Cl^- may occupy over the simulation is represented by the orange mesh. D Side-view of the neck region. F84 of the neck may accommodate for Cl^-; however, the neck is not permeable to Cl^-. E Bottom-up view of F84. Cl^- can be seen to interact with the aromatic ring through edgewise interactions. The coordinating atoms within the first solvation shell of the Cl^- (orange sphere) are represented as spheres.

the PDB structure (Figure 2D) with a distance of 0.7 Å between them (Figure 2E). For comparison with the existing literature, the distance of the Cl^- to the backbone nitrogen of F80 is 3.6 Å compared with 3.2 Å[36] in the experimental structure (Figure S5). Analysis of Cl^- interactions close to the X739 site observed an occupancy of ∼60% averaged across the two AMOEBA simulations, compared to a low (and difficult to estimate) occupancy of ∼15% in the c36m simulation (Figure S5). Studies of CLC channels have revealed that pore-lining backbone amides can influence ion selectivity and permeation.[4] Therefore, it is feasible that the ion-like density in this experimental structure is not water but a Cl^-. This difference in ion location between the simulation and structural densities could be a result of the imposition of 5-fold symmetry during structural processing, which could marginally shift the cryo-EM density in comparison to allowed asymmetric interaction modes. Conversely, from a simulation perspective, the localization of Cl^- can be force field dependent and conditional on the realism of the model.

To demonstrate the impact of modeling polarizability, equivalent simulations were also performed with the non-polarizable force field, CHARMM36m (c36m) (Figure 2F–H). In contrast to the AMOEBA simulations, these simulations suggest that Cl^- tends to localize with a distance of 4.5 Å between X739 and a distance of 6.0 Å from the backbone nitrogen of F80 and prefers to interact with the backbone NH, the hydroxyl group of S79, and the backbone NH of I78 (Figure 2G). The very short residence time of 0.06 ns and low occupancy in c36m simulations (Figure S5) indicate that this is not a stable binding site, with interactions that are weak and highly transient. This is also reflected in replicas of c36m, where PyLipID does not detect the binding site. Furthermore, no alternative binding conformations within the neck region are detected for c36m simulations. Thus, even though this analysis is limited in nature due to the relative size of the system, it still allows a more direct comparison with experimental observations and demonstrates why the inclusion of polarization is important where possible.

Cl^- Ion Permeation and the Role of Water. Water plays a crucial role in ion channel permeation. The dimensions of the open neck state of bestrophin (Figure 3A,B) suggest the neck is sufficiently large to accommodate a fully hydrated Cl^- (radius ∼4 Å,[38] first hydration shell determined by calculating the RDF of Cl–O of water (Figure S2)); the pore is wetted and permeable to ions. However, we observe that permeation through the neck occurs concurrently with the stripping of 1–2 water molecules from the first hydration shell of the ion (Figure 3C). The removal of water molecules allows for direct contact between Cl^- and the hydrophobic aromatic rings. The benzene ring of the phenylalanine has a large negative quadrupole moment that creates a partial negative charge on both faces of the π-system and subsequently a partial positive charge around the edge of the ring.[12,55,56] As a result, the partial loss of hydration of Cl^- can be compensated by favorable interactions with these aromatic rings, which could be regarded as "hydrophobic solvation" (Figure 3E). The

https://doi.org/10.1021/acs.jctc.4c01039
J. Chem. Theory Comput. 2025, 21, 933–942

aromatic side chains of F80 possess rotational freedom, allowing the ring to exist in two main conformations: flipped vertically inward toward the pore axis (Figure 3E) or rotated outward and in a flat orientation (Figure 3F). Both conformations facilitate hydrophobic solvation; however, note that the inward flipped ring conformation occurs from a single protomer. There is no clear correlation between the flipping motion of side chains and interactions with Cl^- in the immediate vicinity.

It has been hypothesized[35−37,54] that such a mechanism may mediate the stabilization of a dehydrated Cl^- at F80 and F84 through anion−π interactions based on the initial X-ray structure of chicken Best1 (cBest1), although this structure was later determined to be in the closed conformation. Mutagenesis studies of the cBest1 neck residues to alanine later showed no effect on ion selectivity and suggested that the role of aromatic side chain interactions may reduce the energy barriers for Cl^- and other anions to permeate the neck region but not be the determining factor for charge selectivity.[57,58] Other forms of hydrophobic solvation mechanisms have previously been observed in simulations of a biomimetic nanopore[59] and a hydrophobic protein binding site[52] whereby Cl^- moved through pores by partially dehydrating and forming energetically favorable interactions with hydrophobic contacts.

Importantly, these anion-hydrophobic interactions were only observed when electronic polarization was included in the molecular model and are not observed in equivalent simulations of the open state hBest1 when using fixed-charge (c36m) descriptions. We attribute this to the fact that anion interactions with aromatic side chains arise mainly from two factors: electrostatic interactions of the quadrupole moment and ion-induced polarization,[56] the latter of which is not captured in c36m.[60]

Analysis of the Partially Open Neck State. The partially open structure of hBest1 presents a more constricted neck region (Figure 1E,G). Critical conformational changes occur in residues F282, F283, and F276 concomitant with changes in neck residues I76, F80, and F84. I76 remains facing away from the pore axis as in the fully open state, while residues F80 and F84 and the hydrophobic gating apparatus adopt a closed-like conformation (Figure 1G).[36] In the experimental structure, an ion-like density is consistently captured at the edge of F84, even when processed with C1 refinement (Figure S1D from[36] i.e., with no symmetry applied. This density could potentially represent a chemical constituent of the buffer system, in which Cl^- is the predominant ion, and so may represent a dehydrated Cl^-. Furthermore, asymmetry in the neck can be observed as a continuous movement between the closed and intermediate states in this region.

Trajectories of ions and water in the partially open state protein fragment (Figure 4A) show traces of Cl^- occupying locations just above F84 in the z-direction. This suggests that F84 is capable of accommodating Cl^-; however, the pore is functionally closed as ions are not conducted across the neck, primarily due to the tight constriction formed by F80. Additionally, a small, transiently dewetted region can be found within the neck between residues (S79 and F80), which reiterates that the partially open state is functionally closed (Figure 4A). Similar behavior is also observed in a replica simulation (Figure S7). The total average number of water molecules in the partially open permeation pathway is ~700 ± 20, as calculated by CHAP.[50] Compared with the fully open state (see above), this reduced number of water molecules indicates a smaller pore volume and suggests the presence of a dewetted region.

The space that Cl^- can occupy is more clearly depicted in Figures 4C,D, where the orange mesh illustrates the volume of space that Cl^- occupies throughout the simulation. The majority of the neck region is devoid of Cl^- which could be associated with the dewetted region, since pore hydration acts as a precursor to ion permeation (Figure 4D). Mutagenesis studies have demonstrated that the conserved "IFF" motif of the neck acts as an effective gate, rather than a selectivity filter, because ionic selectivity remained constant in the mutant channel[57,61] which is in agreement with our results, although we did not perform mutagenesis simulations. F84 accommodates a Cl^- through a mechanism similar to that seen in the previous section: the Cl^- partially dehydrates (Figure S6) to directly interact with up to 2 adjacent pore-facing phenylalanines simultaneously, mediated by their edgewise interaction with the partially dehydrated anion (Figure 4E). Together, these observations support the provisional functional annotation of the channel as "partially open," i.e., it is indeed on the way to either opening or closing, with the neck containing a consistently dewetted region and thus still presenting a barrier to ion permeation even though the neck (F84) can accommodate Cl^-.

This barrier to ion permeation is not necessarily due to steric occlusion but rather to the inability of the Cl^- to shed more of the first hydration shell. The partially open neck is wide enough to accommodate a dehydrated Cl^- (Figure 4A,B) but it is energetically unfavorable to lose more than ~2−3 water molecules in the neck region at the tightest constriction, which would be required for permeation, and therefore ions do not pass through this region. For comparison, in the absence of polarization, c36m simulations suggest the neck is functionally closed, and there is a significantly more prominent dewetted region between S79 and F80. F84 does not accommodate Cl^- but water can occupy this region (Figure 4B).

CONCLUSIONS

We have performed MD simulations of the neck region of hBest1 channels in the open and partially open neck states using a fully polarizable force field (AMOEBA). Our results demonstrate that electronic polarization plays a key role in Cl^- accumulation at the helix dipole (the backbone nitrogen of F80) in the open state, with significant overlap with an ion-like density previously assigned to a water molecule in the cryo-EM structure. Together, our data suggest that this location functions as a Cl^- binding site that contributes to the anion selectivity in the open neck conformation of bestrophins. In contrast, fixed charge (c36m) simulations predict a different location for Cl^- accumulation that is not supported by experimental data, and interactions are more transient, thus underscoring the importance of force field choice in simulation-based functional annotation of polarizable systems. Cl^- permeation through the open neck region is facilitated by edgewise anion interactions with the aromatic side chains of F80, where, again, the influence of electronic polarization appears to exert decisive influence over the functional state of the channel. Simulations of the partially open neck state also support this permeation mechanism, as neck dilation at F84 is able to accommodate Cl^-; however, the pore remains functionally closed and is therefore "partially open". Conversely, c36m simulations predict this 8D1K structure to be functionally closed. This study therefore provides new insights

https://doi.org/10.1021/acs.jctc.4c01039
J. Chem. Theory Comput. 2025, 21, 933−942

into bestrophin channel function, although further studies (e.g., mutagenesis, functional and simulation studies of F84) are required to separate the individual contributions of structural elements to Cl^- permeation and selectivity within the ion pathway.

Overall, our results demonstrate the importance of modeling polarization in situations where polarizable moieties play an essential role in protein function. Appropriate treatment of electrostatics reveals more physically accurate behavior and provides new mechanistic insights into Cl^- permeation. MD simulations employing explicit polarization can, therefore, complement cryo-EM and other structural techniques in the identification and assignment of ambiguous nonprotein densities such as anions.

■ ASSOCIATED CONTENT

Data Availability Statement

The coordinates for full protein structures of hBest1 are available in the RCSB Protein Data Bank (PDB) under ID codes 8D1O for the open state, 8D1K for the partially open state, and 8D1I for the closed state structures. Coordinates for the protein fragment structures used in this article are available at DOI: 10.5281/zenodo.13946753. Nonpolarizable simulations were performed using standard GROMACS protocols, and AMOEBA simulations used OpenMM following the protocol published at https://github.com/Inniag/openmm-scripts-amoeba.[6] PyLipID, used for binding site identification, can be found at https://github.com/wlsong/PyLipID.[47]

Supporting Information

The Supporting Information is available free of charge at https://pubs.acs.org/doi/10.1021/acs.jctc.4c01039.

Full protein embedded simulations; protein fragment system used in simulations; radial distribution functions (RDFs), $gCl^-{-}O(r)$, of water oxygen atoms around a Cl^- ion in bulk solution with the c36m and AMOEBA forcefields; protein fragment system validation; trajectories of molecules in c36m simulation; AMOEBA simulation replica; First hydration shell number of chloride ions in the partially open state structure (PDB ID 8D1K) in bulk (blue) compared with at the z-position corresponding to F84 (orange) within the pore in the AMOEBA simulation; replica AMOEBA simulation (of Figure 4A main text) showing trajectories of molecules (PDF)

■ AUTHOR INFORMATION

Corresponding Author

Stephen J. Tucker − *Department of Physics, Clarendon Laboratory, University of Oxford, Oxford OX1 3PU, U.K.; Kavli Institute for Nanoscience Discovery, University of Oxford, Oxford OX1 3QU, U.K.;* orcid.org/0000-0001-8996-2000; Email: stephen.tucker@physics.ox.ac.uk

Authors

Linda X. Phan − *Department of Physics, Clarendon Laboratory, University of Oxford, Oxford OX1 3PU, U.K.; Department of Biochemistry, University of Oxford, Oxford OX1 3QU, U.K.*

Aaron P. Owji − *Department of Ophthalmology, Columbia University, New York, New York 10032, United States; Department of Pharmacology, Columbia University, New York, New York 10032, United States; Simons Electron Microscopy Center, New York Structural Biology Center, New York, New York 10027, United States*

Tingting Yang − *Department of Ophthalmology, Columbia University, New York, New York 10032, United States*

Jason Crain − *Department of Biochemistry, University of Oxford, Oxford OX1 3QU, U.K.; IBM Research Europe, Hartree Centre, Daresbury WA4 4AD, U.K.;* orcid.org/0000-0001-8672-9158

Mark S.P. Sansom − *Department of Biochemistry, University of Oxford, Oxford OX1 3QU, U.K.*

Complete contact information is available at: https://pubs.acs.org/10.1021/acs.jctc.4c01039

Author Contributions

All authors designed the research and wrote the paper. L.X.P. performed the research and analyzed the data. S.J.T., J.C., M.S.P.S., and T.Y. obtained funding for the project.

Notes

The authors declare the following competing financial interest(s): JC is an employee of IBM Research.

■ ACKNOWLEDGMENTS

We thank T. Bertie Ansell for their insightful discussions regarding the analysis and usage of PylipID. We would like to acknowledge the ARCHER2 UK National Supercomputing Service (http://www.archer2.ac.uk) and the University of Oxford Advanced Research Computing (ARC) facility for their support in carrying out this work (10.5281/zenodo.22558). This work was supported by grants from the Biotechnology and Biological Sciences Research Council, the Engineering and Physical Sciences Research Council, and National Institutes of Health grant R35GM149252.

■ REFERENCES

(1) Hille, B.; *Ionic Channels of Excitable Membranes*, 3rd ed.; Sinauer Associates Inc., 2001.

(2) Roux, B. Ion Channels and Ion Selectivity. *Essays Biochem.* **2017**, *61* (2), 201−209.

(3) Ashcroft, F.; *Ion Channels and Disease* Academic Press, 2000.

(4) Leisle, L.; Lam, K.; Dehghani-Ghahnaviyeh, S.; Fortea, E.; Galpin, J. D.; Ahern, C. A.; Tajkhorshid, E.; Accardi, A. Backbone Amides Are Determinants of Cl− Selectivity in CLC Ion Channels. *Nat. Commun.* **2022**, *13* (1), 1−11.

(5) Garrett, B. C. Ions at the Air/Water Interface. *Science* **2004**, *303* (5661), 1146−1147.

(6) Klesse, G.; Rao, S.; Tucker, S. J.; Sansom, M. S. P. Induced Polarization in Molecular Dynamics Simulations of the 5-HT3 Receptor Channel. *J. Am. Chem. Soc.* **2020**, *142* (20), 9415−9427.

(7) Hantal, G.; Kolafa, J.; Sega, M.; Jedlovszky, P. Single-Particle Dynamics at the Intrinsic Surface of Aqueous Alkali Halide Solutions. *J. Phys. Chem. B* **2021**, *125* (2), 665−679.

(8) Petersen, P. B.; Saykally, R. J. On the Nature of Ions at the Liquid Water Surface. *Annu. Rev. Phys. Chem.* **2006**, *57* (1), 333−364.

(9) Bajaj, P.; Riera, M.; Lin, J. K.; Mendoza Montijo, Y. E.; Gazca, J.; Paesani, F. Halide Ion Microhydration: Structure, Energetics, and Spectroscopy of Small Halide-Water Clusters. *J. Phys. Chem. A* **2019**, *123* (13), 2843−2852.

(10) Gale, P. A. Anion Receptor Chemistry. *Chem. Commun.* **2011**, *47* (1), 82−86.

(11) Chakravarty, S.; Ung, A. R.; Moore, B.; Shore, J.; Alshamrani, M. A Comprehensive Analysis of Anion-Quadrupole Interactions in Protein Structures. *Biochemistry* **2018**, *57* (12), 1852−1867.

(12) Jackson, M. R.; Beahm, R.; Duvvuru, S.; Narasimhan, C.; Wu, J.; Wang, H. N.; Philip, V. M.; Hinde, R. J.; Howell, E. E. A Preference for Edgewise Interactions between Aromatic Rings and Carboxylate

Anions: The Biological Relevance of Anion-Quadrupole Interactions. *J. Phys. Chem. B* **2007**, *111* (28), 8242−8249.
(13) Breberina, L. M.; Milčić, M. K.; Nikolić, M. R.; Stojanović, S. D. Contribution of Anion-π Interactions to the Stability of Sm/LSm Proteins. *J. Biol. Inorg. Chem.* **2015**, *20* (3), 475−485.
(14) Jojoa-Cruz, S.; Saotome, K.; Tsui, C. C. A.; Lee, W. H.; Sansom, M. S. P.; Murthy, S. E.; Patapoutian, A.; Ward, A. B. Structural Insights into the Venus Flytrap Mechanosensitive Ion Channel Flycatcher1. *Nat. Commun.* **2022**, *13* (850), 1−11.
(15) Chen, Y. H.; Hu, L.; Punta, M.; Bruni, R.; Hillerich, B.; Kloss, B.; Rost, B.; Love, J.; Siegelbaum, S. A.; Hendrickson, W. A. Homologue Structure of the SLAC1 Anion Channel for Closing Stomata in Leaves. *Nature* **2010**, *467* (7319), 1074−1080.
(16) Deng, Z.; Maksaev, G.; Schlegel, A. M.; Zhang, J.; Rau, M.; Fitzpatrick, J. A. J.; Haswell, E. S.; Yuan, P. Structural Mechanism for Gating of a Eukaryotic Mechanosensitive Channel of Small Conductance. *Nat. Commun.* **2020**, *11* (1), 1−9.
(17) Renaud, J. P.; Chari, A.; Ciferri, C.; Liu, W. T.; Rémigy, H. W.; Stark, H.; Wiesmann, C. Cryo-EM in Drug Discovery: Achievements, Limitations and Prospects. *Nat. Rev. Drug Discovery* **2018**, *17* (7), 471−492.
(18) D'Imprima, E.; Kühlbrandt, W. Current Limitations to High-Resolution Structure Determination by Single-Particle CryoEM. *Q. Rev. Biophys.* **2021**, *54* (e4), 1−15.
(19) Beckers, M.; Mann, D.; Sachse, C. Structural Interpretation of Cryo-EM Image Reconstructions. *Prog. Biophys. Mol. Biol.* **2021**, *160*, 26−36.
(20) Nierzwicki, Ł.; Palermo, G. Molecular Dynamics to Predict Cryo-EM: Capturing Transitions and Short-Lived Conformational States of Biomolecules. *Front. Mol. Biosci.* **2021**, *8*, 1−6.
(21) Lopes, P. E. M.; Roux, B.; MacKerell, A. D. Molecular Modeling and Dynamics Studies with Explicit Inclusion of Electronic Polarizability: Theory and Applications. *Theor. Chem. Acc.* **2009**, *124* (1−2), 11−28.
(22) Nencini, R.; Tempra, C.; Biriukov, D.; Riopedre-Fernandez, M.; Chamorro, V. C.; Polák, J.; Mason, P. E.; Ondo, D.; Heyda, J.; Samuli Ollila, O. H.; et al. Effective Inclusion of Electronic Polarization Improves the Description of Electrostatic Interactions: The ProsECCo75 Biomolecular Force Field. *J. Chem. Theory Comput.* **2024**, *20*, 7546−7559.
(23) Duboue-Dijon, E.; Javanainen, M.; Delcroix, P.; Jungwirth, P.; Martinez-Seara, H. A Practical Guide to Biologically Relevant Molecular Simulations with Charge Scaling for Electronic Polarization. *J. Chem. Phys.* **2020**, *153*, 050901.
(24) Kohagen, M.; Lepšík, M.; Jungwirth, P. Calcium Binding to Calmodulin by Molecular Dynamics with Effective Polarization. *J. Phys. Chem. Lett.* **2014**, *5* (22), 3964−3969.
(25) Tolmachev, D. A.; Boyko, O. S.; Lukasheva, N. V.; Martinez-Seara, H.; Karttunen, M. Overbinding and Qualitative and Quantitative Changes Caused by Simple Na+ and K+ Ions in Polyelectrolyte Simulations: Comparison of Force Fields with and without NBFIX and ECC Corrections. *J. Chem. Theory Comput.* **2020**, *16* (1), 677−687.
(26) Orabi, E. A.; Öztürk, T. N.; Bernhardt, N.; Faraldo-Gómez, J. D. Corrections in the CHARMM36 Parametrization of Chloride Interactions with Proteins, Lipids, and Alkali Cations, and Extension to Other Halide Anions. *J. Chem. Theory Comput.* **2021**, *17* (10), 6240−6261.
(27) Ponder, J. W.; Wu, C.; Ren, P.; Pande, V. S.; Chodera, J. D.; Schnieders, M. J.; Haque, I.; Mobley, D. L.; Lambrecht, D. S.; Distasio, R. A.; Head-Gordon, M.; Clark, G. N. I.; Johnson, M. E.; Head-Gordon, T. Current Status of the AMOEBA Polarizable Force Field. *J. Phys. Chem. B* **2010**, *114* (8), 2549−2564.
(28) Huang, J.; Lopes, P. E. M.; Roux, B.; MacKerell, A. D. Recent Advances in Polarizable Force Fields for Macromolecules: Microsecond Simulations of Proteins Using the Classical Drude Oscillator Model. *J. Phys. Chem. Lett.* **2014**, *5* (18), 3144−3150.
(29) Ngo, V.; Li, H.; MacKerell, A. D.; Allen, T. W.; Roux, B.; Noskov, S. Polarization Effects in Water-Mediated Selective Cation Transport across a Narrow Transmembrane Channel. *J. Chem. Theory Comput.* **2021**, *17* (3), 1726−1741.
(30) Deng, J.; Cui, Q. Electronic Polarization Leads to a Drier Dewetted State for Hydrophobic Gating in the Big Potassium Channel. *J. Phys. Chem. Lett.* **2024**, *15*, 7436−7441.
(31) Peng, X.; Zhang, Y.; Chu, H.; Li, Y.; Zhang, D.; Cao, L.; Li, G. Accurate Evaluation of Ion Conductivity of the Gramicidin A Channel Using a Polarizable Force Field without Any Corrections. *J. Chem. Theory Comput.* **2016**, *12* (6), 2973−2982.
(32) Okur, H. I.; Hladílková, J.; Rembert, K. B.; Cho, Y.; Heyda, J.; Dzubiella, J.; Cremer, P. S.; Jungwirth, P. Beyond the Hofmeister Series: Ion-Specific Effects on Proteins and Their Biological Functions. *J. Phys. Chem. B* **2017**, *121* (9), 1997−2014.
(33) Rao, S.; Klesse, G.; Stansfeld, P. J.; Tucker, S. J.; Sansom, M. S. P. A BEST Example of Channel Structure Annotation by Molecular Simulation. *Channels* **2017**, *11* (4), 347−353.
(34) Owji, A. P.; Kittredge, A.; Zhang, Y.; Yang, T. Structure and Function of the Bestrophin Family of Calcium-Activated Chloride Channels. *Channels* **2021**, *15* (1), 604−623.
(35) Yang, T.; Liu, Q.; Kloss, B.; Bruni, R.; Kalathur, R. C.; Guo, Y.; Kloppmann, E.; Rost, B.; Colecraft, H. M.; Hendrickson, W. A. Structure and Selectivity in Bestrophin Ion Channels. *Science* **2014**, *346* (6207), 355−359.
(36) Owji, A. P.; Wang, J.; Kittredge, A.; Clark, Z.; Zhang, Y.; Hendrickson, W. A.; Yang, T. Structures and Gating Mechanisms of Human Bestrophin Anion Channels. *Nat. Commun.* **2022**, *13* (3836), 1−11.
(37) Owji, A. P.; Zhao, Q.; Ji, C.; Kittredge, A.; Hopiavuori, A.; Fu, Z.; Ward, N.; Clarke, O. B.; Shen, Y.; Zhang, Y.; Hendrickson, W. A.; Yang, T. Structural and Functional Characterization of the Bestrophin-2 Anion Channel. *Nat. Struct. Mol. Biol.* **2020**, *27* (4), 382−391.
(38) Zhao, Z.; Rogers, D. M.; Beck, T. L. Polarization and Charge Transfer in the Hydration of Chloride Ions. *J. Chem. Phys.* **2010**, *132* (1), 1−10.
(39) Jo, S.; Kim, T.; Iyer, V. G.; Im, W. CHARMM-GUI: A Web-Based Graphical User Interface for CHARMM. *J. Comput. Chem.* **2008**, *29* (11), 1859−1865.
(40) Abraham, M. J.; Murtola, T.; Schulz, R.; Páll, S.; Smith, J. C.; Hess, B.; Lindah, E. Gromacs: High Performance Molecular Simulations through Multi-Level Parallelism from Laptops to Supercomputers. *SoftwareX* **2015**, *1−2*, 19−25.
(41) Evans, D. J.; Holian, B. L. The Nose-Hoover Thermostat. *J. Chem. Phys.* **1985**, *83* (8), 4069−4074.
(42) Parrinello, M.; Rahman, A. Polymorphic Transitions in Single Crystals: A New Molecular Dynamics Method. *J. Appl. Phys.* **1981**, *52* (12), 7182−7190.
(43) Essmann, U.; Perera, L.; Berkowitz, M. L.; Darden, T.; Lee, H.; Pedersen, L. G. A Smooth Particle Mesh Ewald Method. *J. Chem. Phys.* **1995**, *103* (19), 8577−8593.
(44) Hess, B.; Bekker, H.; Berendsen, H. J. C.; Fraaije, J. G. E. M. LINCS: A Linear Constraint Solver for Molecular Simulations. *J. Comput. Chem.* **1997**, *18*, 1463−1472.
(45) Shi, Y.; Xia, Z.; Zhang, J.; Best, R.; Wu, C.; Ponder, J. W.; Ren, P. Polarizable Atomic Multipole-Based AMOEBA Force Field for Proteins. *J. Chem. Theory Comput.* **2013**, *9* (9), 4046−4063.
(46) Tuckermar, M.; Berne, B. J.; Martyna, G. J. Reversible Multiple Time Scale Molecular Dynamics. *J. Chem. Phys.* **1992**, *97* (3), 1990−2001.
(47) Song, W.; Corey, R. A.; Ansell, T. B.; Cassidy, C. K.; Horrell, M. R.; Duncan, A. L.; Stansfeld, P. J.; Sansom, M. S. P. PyLipID: A Python Package for Analysis of Protein-Lipid Interactions from Molecular Dynamics Simulations. *J. Chem. Theory Comput.* **2022**, *18* (2), 1188−1201.
(48) Gowers, R. J.; Linke, M.; Barnoud, J.; Reddy, T.; John, E.; Melo, M. N.; Seyler, S. L.; Domanski, J.; Dotson, D. L.; Buchoux, S.; et al. MDAnalysis: A Python Package for the Rapid Analysis of Molecular Dynamics Simulations. *Proceedings of the 15th Python in*

https://doi.org/10.1021/acs.jctc.4c01039
J. Chem. Theory Comput. 2025, 21, 933−942

Science Conference Los Alamos National Laboratory (LANL), 2016, pp 98−105.
(49) Michaud-Agrawal, N.; Denning, E. J.; Woolf, T. B.; Beckstein, O. MDAnalysis: A Toolkit for the Analysis of Molecular Dynamics Simulations. *J. Comput. Chem.* **2011**, *32* (10), 2319−2327.
(50) Klesse, G.; Rao, S.; Sansom, M. S. P.; Tucker, S. J. CHAP: A Versatile Tool for the Structural and Functional Annotation of Ion Channel Pores. *J. Mol. Biol.* **2019**, *431* (17), 3353−3365.
(51) Klesse, G.; Tucker, S. J.; Sansom, M. S. P. Electric Field Induced Wetting of a Hydrophobic Gate in a Model Nanopore Based on the 5-HT3 Receptor Channel. *ACS Nano* **2020**, *14* (8), 10480−10491.
(52) Phan, L. X.; Chamorro, V. C.; Martinez-Seara, H.; Crain, J.; Sansom, M. S. P.; Tucker, S. J. Influence of Electronic Polarization on the Binding of Anions to a Chloride-Pumping Rhodopsin. *Biophys. J.* **2023**, *122* (8), 1548−1558.
(53) Hol, W. G. J.; van Duijnen, P. T.; Berendsen, H. J. The α-helix dipole and the properties of proteins. *Nature* **1978**, *273* (5662), 443−446.
(54) Dickson, V. K.; Pedi, L.; Long, S. B. Structure and Insights into the Function of a Ca2+-Activated Cl- Channel. *Nature* **2014**, *516* (7530), 213−218.
(55) Dhotel, A.; Chen, Z.; Delbreilh, L.; Youssef, B.; Saiter, J. M.; Tan, L. Molecular Motions in Functional Self-Assembled Nanostructures. *Int. J. Mol. Sci.* **2013**, *14* (2), 2303−2333.
(56) Kan, X.; Liu, H.; Pan, Q.; Li, Z.; Zhao, Y. Anion-π Interactions: From Concept to Application. *Chin. Chem. Lett.* **2018**, *29* (2), 261−266.
(57) Vaisey, G.; Miller, A. N.; Long, S. B. Distinct Regions That Control Ion Selectivity and Calcium-Dependent Activation in the Bestrophin Ion Channel. *Proc. Natl. Acad. Sci. U. S. A.* **2016**, *113* (47), No. e7399−e7408.
(58) Miller, A. N.; Vaisey, G.; Long, S. B. Molecular Mechanisms of Gating in the Calcium-Activated Chloride Channel Bestrophin. *Elife* **2019**, *8*, No. e43231.
(59) Phan, L. X.; Lynch, C. I.; Crain, J.; Sansom, M. S. P.; Tucker, S. J. Influence of Effective Polarization on Ion and Water Interactions within a Biomimetic Nanopore. *Biophys. J.* **2022**, *121* (11), 2014−2026.
(60) Lin, F. -Y.; MacKerell, A. D., Jr. Improved Modeling of Cation-π and Anion-Ring Interactions Using the Drude Polarizable Empirical Force Field for Proteins. *J. Comput. Chem.* **2020**, *41*, 439−448.
(61) Rao, S.; Lynch, C. I.; Klesse, G.; Oakley, G. E.; Stansfeld, P. J.; Tucker, S. J.; Sansom, M. S. P. Water and Hydrophobic Gates in Ion Channels and Nanopores. *Faraday Discuss.* **2018**, *209*, 231−247.

https://doi.org/10.1021/acs.jctc.4c01039
J. Chem. Theory Comput. 2025, 21, 933−942